CRYSTAL GROWTH OF GYPSUM ON ITS (010)* CLEAVED SURFACE

by

M. GOTO** and M. J. RIDGE***

(with 23 Text-Figures and 3 Plates)

(Contribution from the Department of Geology and Mineralogy, Faculty of Science, Hokkaido University. No. 1055)

1. Introduction

If we cleave a gypsum crystal along its (010) plane, we can observe fine cleaved steps traversing the very clear field of the cleaved surface. The step-lines are found to be mostly of the [101] direction and partly of the [001]; they certainly correspond to the ($\bar{1}01$) and the (100) cleavages, which both are very common in gypsum crystal.

When the cleaved surface is allowed to grow in a solution supersaturated with gypsum, the growth initially takes place at sites of the ($\bar{1}01$) cleaved step, then develops to give the step an irregular, dog-teeth shaped outline of the growth front as shown in *Photo 1*. At sites of the (100) step, on the other hand, the initiation of growth is hardly observed. This characteristic feature of growth on the cleaved (010) surface may suggest a great more predominating tendency of gypsum crystal of growing in the c-axis direction than growing in other directions.

In this paper an attempt was made to explain this special growth pattern by calculating the energies necessary to form an adsorbed atom on various sites of the ($\bar{1}01$) and the (100) steps. The main part of the calculation was done with the aid of electric computer, and the result is thought succeeded in giving a fairly clear picture of changing with time of the energy configurations of the steps, so as to enable us to plot the most probable sequence of adsorption of atoms for the growth of each step.

A basic assumption upon which our calculations were carried on is to let all steps on the (010) cleaved surface be of the mono-atomic height; it was possible for us with this assumption to calculate the energy of any atom at any site of the steps with an enough accuracy, taking the interactions upon the given atom of all

---

* In this paper the morphological axes described by DANA (1915) were used.

** Department of Geology and Mineralogy, Hokkaido University, Sapporo, Japan.

*** Division of Building Research, CSIRO, Melbourne, Australia.

other atoms (not only neighbouring atoms) in the *infinitely large crystal* of gypsum into account.

Since any real steps observable on the sample can not be of the mono-atomic height, the validity of the theory derived from such a simplified model may remain in some doubt when it is applied to the growth process of the real steps, which certainly have multiatomic heights. It is however possible that the overall pattern of growth of a multiatomic step is determined by the growth pattern of the first mono-atomic layer, the growth of which will initiate at the bottom of the multiatomic step. The very good correspondence as seen between the growth pattern actually observed on the sample and the pattern derived from the theory may present a proof of the above mentioned opinion.

2. *Energy of the infinite* Ca-SO_4 *monolayer*

The structure of gypsum may be said, in brief, to be composed of alternating superpositions of Ca-SO_4 layers and H_2O layers; two successively piled Ca-SO_4 mono-atomic layers as an unit and two successively piled H_2O mono-molecular layers as another unit appear alternatingly to form a layer structure, as illustrated in Fig. 1. These layers extend perpendicular to the b-axis of the crystal and give the structure a great cleavability along the (010) plane. Therefore, if we suppose any mono-atomic step on this (010) surface, the *cliff* of the step (simply " the step " hereafter) must be a lateral side of the Ca-SO_4 monolayer or that of the H_2O monolayer (see also Fig. 1).

Of the two kinds of steps mentioned above, the step of the H_2O monolayer seems to hardly bear its importance in the growth process. The dipole-dipole interaction between water molecules and the ion-dipole interaction between an ion and water molecule are generally weaker than the anion-cation interaction, and they decrease with distance more rapidly than the ionic interaction does. It should also be mentioned that a special coordination is required of water molecules for their dipole-dipole interactions to be able to act effectively. The arrangement of the water molecules in the H_2O monolayer in gypsum is far from such a co-ordination requirement.

The facts mentioned above strongly suggest that the H_2O monolayer does not grow by means of successive adsorptions of water molecules on its step-side, or in other words, that the characteristic growth pattern on the cleaved surface could not be a result of *layer growth* of the H_2O monolayer itself. We conclude, therefore, that only the step of the Ca-SO_4 monolayer needs to be taken into consideration when the growth pattern on the (010) cleaved surface is to be examined. The formation of the H_2O monolayer may be a dependent event following the growth of the Ca-SO_4 monolayer.

According to WOOSTER (1936), the atomic arrangement of Ca and SO_4 ions in the Ca-SO_4 monolayer is as shown in Fig. 2. The lattice factors necessary to

describe this arrangement are: a=10.47, c=6.26 Å, and β=98°58′. Now if it be considered that a Ca (or SO_4) ion is at the centre of this monolayer, the positions relative to this central ion of all other ions in the layer can be described as a simple coordinate system by the following equation:

$$d^2 = (5.235\,x)^2+(3.14\,y)^2\pm 32.8758\,xy\cdot\cos(180°-98°58') \quad \text{.....(1)}$$

where the sign for the last term is positive for the ions situated in the first and third quadrants, and negative for those in the second and fourth quadrants. The X_0-axis of the coordinate corresponds to the crystallographic a-axis, and the Y_0-axis to the c-axis. If a given ion is situated, for example, in the first quadrant and belongs to the i-th column (the i-th single Ca-SO_4 chain parallel to the c-axis) and at the same time to the k-th rank (the k-th single Ca-SO_4 chain parallel to the a-axis), the distance between the given ion and the central ion is given as:

$$d = \sqrt{(5.235\,i)^2+(3.14\,k)^2+32.8758\,ik\cdot\cos 81°02'} \quad \text{.....(2)}$$

The interaction among ions in the Ca-SO_4 monolayer is thought to be purely ionic. This means that the potential energy of the central ion in the layer can be given as the total algebraic sum of the electrostatic interactions upon it of all other ions in the layer. The electrostatic interaction between two ions is a function of the reciprocal of the distance between the two ions: $U=\pm f(1/d)$. In this paper we use the value of 1/d, with a proper sign, for the real energy value f(1/d). The conversion from one value to the other is however very simple, because $f(1/d)=4e^2/d.10^{-12}$erg.

For obtaining the total interaction upon the central ion, $\sum'(1/d)$, it is of a mathematical convenience to calculate the interactions from each column and rank separately, then sum them up. In this paper, the electrostatic interaction is signed positive when it acts between Ca^{++} and $SO_4^{=}$, and negative between ions of the same kind, viz. Ca^{++} and Ca^{++} or $SO_4^{=}$ and $SO_4^{=}$. A term $(-1)^n$ or $(-1)^{n+1}$ is used, being combined with the equation (2), to give a proper sign to a given interaction. Thus, the interaction upon the central ion from the second column in the first quadrant, for example, can be given as:

$$U(2C) = \sum_{y=1}^{\infty}\left(\frac{(-1)^{y+1}}{d(y)}\right)_{x=2} \quad \text{.....(3)}$$

The interaction from the third column is in the same way as:

$$U(3C) = \sum_{y=1}^{\infty}\left(\frac{(-1)^{y}}{d(y)}\right)_{x=3} \quad \text{.....(4)}$$

Also, the interactions from the 6th and 7th rank, for examples, are

$$U(6R) = \sum_{x=1}^{\infty} \left(\frac{(-1)^{x+1}}{d(x)} \right)_{y=6} \quad \cdots\cdots(5)$$

and

$$U(7R) = \sum_{x=1}^{\infty} \left(\frac{(-1)^{x}}{d(x)} \right)_{y=7} \quad \cdots\cdots(6)$$

The variables x and y in these equations are confined to take only positive integers of other than zero.

Although it is self-evident that an equation like (3), (4), (5) and (6) converges finally to a definite value, there seems to be no direct solutions of these equations to obtain the final values with a reasonable accuracy. However, we found otherwise a satisfactory way for the purpose, applying the Euler transformation (cf. K. KNOPP, 1928) to them. This method was found to give the final values of these equations without any approximation; it is as follows.

Let assume $(S_n)_{n=1,2,3,\ldots\ldots}$ be a given sequence of real or complex numbers. If we define $S_n^{(0)}=S_n$ and for $k \geqq 1$

$$S_n^{(k)} = \frac{1}{2}\left\{ \frac{S_n^{(k-1)}+S_{n+2}^{(k-1)}}{2} + S_{n+1}^{(k-1)} \right\},$$

then we have*

$$S_n^{(k)} = \frac{1}{2^{2k}} \sum_{i=0}^{2k} \binom{2k}{i} S_{n+i}$$

for $k \geqq 0$ and $n=1,2,3,\ldots\ldots$ The term $\binom{2k}{i}$ in the above equation denotes the binomial coefficient as

$$\binom{2k}{i} = \frac{(2k)!}{i!\,(2k-i)!}.$$

The new sequence, $S_n^{(k)}$; $k \geqq 1$, thus obtained is known to be an Euler transformation of the sequence (S_n). We have then the following result:

If the sequence (S_n) is convergent, i.e. if the limit $\lim_{n\to\infty}(S_n)$ exists**, then

(1) for every fixed k we have $\lim_{n\to\infty} S_n^{(k)} = \lim_{n\to\infty} S_n$, and

(2) for every fixed m we have $\lim_{k\to\infty} S_m^{(k)} = \lim_{n\to\infty} S_n$.

The following is an example of how this method (E.T.M. hereafter) is applied

* This can be easily proved by induction on K.

** In the present case the existence of the limit is self-evident.

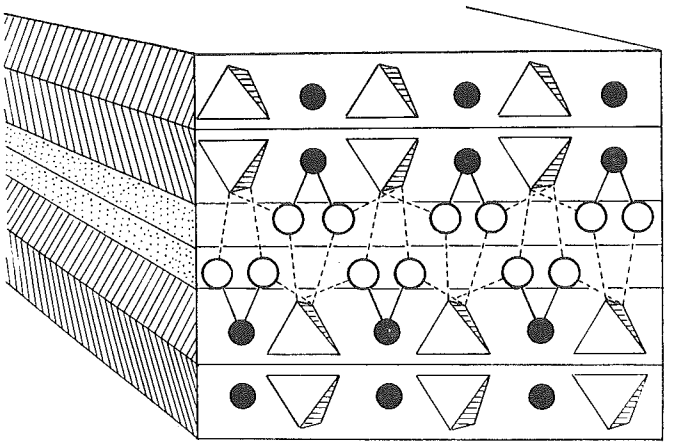

Fig. 1
Schematic illustration of the layer structure of gypsum, showing a section parallel to the (001). The solid circles denote the positions of Ca, the open circles those of water molecules, and the tetrahedrons SO_4.

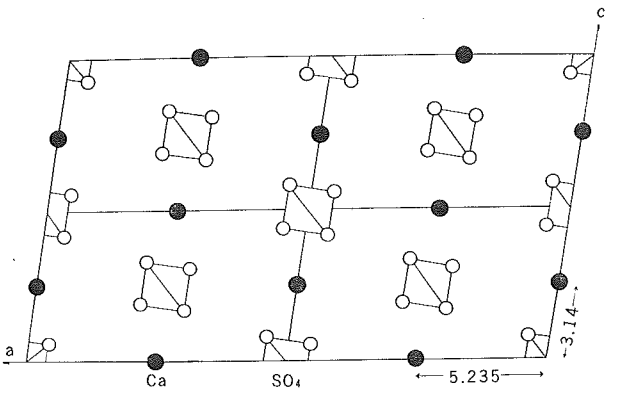

Fig. 2
Arrangements of Ca and SO_4 ions in the layer parallel to the (010).

to the calculation of the interaction from a given Ca-SO_4 chain (column or rank). Suppose the given chain be the first rank in the fourth quadrant; $1\bar{R}$ ($x=1—\infty$, $y=\bar{1}$). The distance between the central ion and the i-th ion in this $1\bar{R}$ rank, viz. the ion that has the coordination of ($x=i$, $y=\bar{1}$), is given according to the equation (2) as:

$$d_i = \sqrt{(5.235i)^2+(3.14)^2-32.8758i\cdot\cos 81°02'} \quad \text{.....(7)}$$

The electrostatic interaction between the two ions is given as $(-1)^i/d_i$ (this value

is used, as mentioned before, for the real energy value), and the whole interaction from the $1\bar{R}$ rank upon the central ion is then given according to the equation (6) as:

$$U(1\bar{R}) = \sum_{i=0}^{\infty}\left(\frac{(-1)^i}{d_i}\right), \quad i = 1, 2, 3, \ldots\ldots\ldots\ldots$$

The values of $(-1)^x/d_x$ for the $1\bar{R}$ rank were calculated for $x=1$ to 20, which are shown in the first column of Table 1. The values of $\sum_{x=1}^{x}(-1)^x/d_x$ for the same range of x are shown in the second column. The values $\sum_{x=1}^{x}(-1)^x/d_x$ form a sequence of real numbers which evidently is convergent. Therefore if we define

$$\sum_{x=1}^{x}\left(\frac{(-1)^x}{d_x}\right) = S_x^{(0)} = S_x\,,$$

the sequences obtained by Euler transformation, such as

$$S_x^{(1)} = \frac{1}{2}\times\left\{\frac{S_x+S_{x+2}}{2}+S_{x+1}\right\},$$

$$S_x^{(2)} = \frac{1}{2}\times\left\{\frac{S_x^{(1)}+S_{x+2}^{(1)}}{2}+S_{x+1}^{(1)}\right\}, \text{ and}$$

$$S_x^{(3)} = \frac{1}{2}\times\left\{\frac{S_x^{(2)}+S_{x+2}^{(2)}}{2}+S_{x+1}^{(2)}\right\}, \text{ and so on,}$$

will also be convergent and have the same final value as of the original sequence $S_x^{(0)}$. It is easily proved that a sequence of higher transformation converges to the final value more quickly than a sequence of lower transformation, that is, $S_x^{(3)}$ converges more quickly than $S_x^{(2)}$ does, and much more quickly than $S_x^{(1)}$ does. This means that we can obtain the final value $\sum_{i=1}^{\infty}(-1)^i/d_i$ simply by two or three transformations of a limited sequence consisting usually of less than twenty numbers. This situation can be seen clearly in Table 1.

In order to check the reliability of the E.T.M., the values of $S_x^{(0)}$ were calculated up to $x=501$ for some arbitrarily chosen columns and ranks, then the values of $1/2\,(S_{500}+S_{501})$ were compared with the corresponding final values obtained by E.T.M. The correspondences are very satisfactory as seen in Table 2. The columns and ranks chosen are the first and the 10th rank in the first (or the third) quadrant and the first and the 10th column in the second (or the fourth) quadrant.

Table 1. Convergency patterns of $S_x^{(0)}$, $S_x^{(1)}$, $S_x^{(2)}$, and $S_x^{(3)}$ of the first rank in the 2nd (or 4th) quadrant ($1\bar{R}$).

	$\frac{(-1)^x}{d_x}$	$\sum_{x=1}^{x}\frac{(-1)^x}{d_x}=S_x^{(0)}$	$S_x^{(1)}$	$S_x^{(2)}$	$S_x^{(3)}$
x=1	−0.176389				
2	+0.095681	−0.080708			
3	−0.064398	−0.145106	−0.116921		
4	+0.048345	−0.096761	−0.118510	−0.117912	
5	−0.038652	−0.135413	−0.117705	−0.118022	−0.117984
6	+0.032179	−0.103234	−0.118168	−0.117980	−0.117995
7	−0.027557	−0.130791	−0.117879	−0.117999	−0.117992
8	+0.024093	−0.106698	−0.118071	−0.117989	−0.117993
9	−0.021400	−0.128098	−0.117936	−0.117994	−0.117992
10	+0.019248	−0.108850	−0.118034	−0.117991	−0.117993
11	−0.017489	−0.126339	−0.117961	−0.117993	−0.117993
12	+0.016024	−0.110315	−0.118017	−0.117992	−0.117993
13	−0.014785	−0.125100	−0.117973	−0.117993	−9.117993
14	+0.013724	−0.111376	−0.118008	−0.117992	−0.117993
15	−0.012805	−0.124181	−0.117980	−0.117993	−0.117993
16	+0.012001	−0.112180	−0.118003	−0.117993	−0.117993
17	−0.011292	−0.123472	−0.117984	−9.117993	
18	+0.010662	−0.112810	−0.118001		
19	−0.010099	−0.122909			
20	+0.009592				

Final value; $U\text{-}1\bar{R}=-0.117993$

They are denoted as 1R, 10R, $1\bar{C}$ and $10\bar{C}$ respectively in the table. The value $1/2(S_{500}+S_{501})$ does by no means correspond exactly to the final value of $\sum S_x$, but may be very close to it because of such a large value of x as 500.

Table 2. Accuracy estimation of Euler transformation method for arbitrarily chosen sequences.

Column and rank chosen.	S_{500}	S_{501}	$\frac{1}{2}(S_{500}+S_{501})$	$\sum_{x=1}^{\infty}S_x$ by E.T.M.
1R	−0.1004684	−0.1008496	−0.1006590	−0.1006597
10R	+0.0155218	+0.0159023	+0.0157120	+0.0157125
$1\bar{C}$	−0.0995103	−0.1001463	−0.0998283	−0.0998285
$10\bar{C}$	+0.0092762	+0.0099148	+0.0095955	+0.0095957

The same procedure as employed for obtaining the interaction from a given chain (column or rank) upon the central ion can also be applied to obtain the whole interaction from a given quadrant. As to the overall interaction from the first quadrant to the central ion, for example, we reasonably assume that the sequence

$\sum U(iC)$, i=1,2,3,..... is also convergent and has a final value which corresponds to the interaction of the first quadrant. A repeated Euler transformation gave the final value as −0.060090, as shown in Table 3.

Table 3. Euler transformations of the sequence $\sum_{i=1}^{i} U(iC)$.

Column (x=i, y=1−∞)	U(xC)	$S_x^{(0)} = \sum_{x=1}^{x} U(xC)$	$S_x^{(1)}$	$S_x^{(2)}$	$S_x^{(3)}$
1st (x=1, y=1−∞)	−0.08853	−0.08853			
2nd (2, „)	+0.04654	−0.04199	−0.06145		
3rd (3, „)	−0.03132	−0.07331	−0.05951	−0.06024	
4th (4, „)	+0.02360	−0.04971	−0.06034	−0.06005	−0.06011
5 „ (5, „)	−0.01892	−0.06863	−0.05995	−0.06010	−0.06009
6 „ (6, „)	+0.01579	−0.05284	−0.06017	−0.06008	−0.06009
7 „ (7, „)	−0.01355	−0.06639	−0.06003	−0.06009	−0.060090
8 „ (8, „)	+0.01187	−0.05452	−0.06013	−0.06009	−0.060090
9 „ (9, „)	−0.01056	−0.06508	−0.06006	−0.06009	−0.060090
10 „ (10, „)	+0.00951	−0.05557	−0.06011	−0.06009	
11 „ (11, „)	−0.00865	−0.06422	−0.06007		
12 „ (12, „)	+0.00793	−0.05629			

U(1Q)=−0.060090

The same value for the interaction from the first quadrant must also be obtained by Euler transformations of $\sum U(iR)$, instead of $\sum U(iC)$. In other words, the interaction from a given quadrant can be obtained by summing up either the interactions from every column or those from every rank in the quadrant. The value obtained by $\sum U(iR)$ was found to be -0.060098, which is in good agreement with that from $\sum U(iC)$. The small difference, 0,000008, between the two values seems to be natural, considering the number of the figures taken for the calculation.

The interaction from the second quadrant was found in the same way to be −0.069635. The position of the third quadrant as to the central ion is symmetrically equivalent to the first quadrant, so the third quadrant yields the same amount of interaction as that of the first quadrant. The same relation is held between the second and fourth quadrants. Besides those from the four quadrants mentioned above, there are interactions to the central ion from the four basic chains which correspond to the coordinate axes; the $+X_0$, $-X_0$, $+Y_0$ and $-Y_0$ chains. Obviously the interactions from the $+Y_0$ and $-Y_0$ chains (the 0- and $\bar{0}$-column respectively) are of the same value, and given as $U(0C)=U(\bar{0}C)=(\log 2)/3.14=+0.220748$. Similarly the interactions from the $+X_0$ and $-X_0$ chains (the 0- and $\bar{0}$-rank) are given as $U(0R)=U(\bar{0}R)=+(\log 2)/5.235=+0.132406$.

Now, the entire energy of the central ion of the Ca-SO_4 monolayer can be obtained as the algebraic sum of the electrostatic interactions from the four quad-

rants and the four basic chains as:

$$U_0 = 2\,(0.220748 + 0.132406 - 0.060090 - 0.069635)$$
$$= +0.446842$$

where, as already mentioned, the interactions are signed positive when they are the attractive interaction, and negative when repulsive. Therefore, one should know that a given ion is stable if its energy has a positive value and unstable if negative value. The allocation pattern, through the infinite Ca-SO_4 monolayer, of the energy of the central ion is illustrated in Fig. 3, where (and also hereafter in this paper) the energy values are given as the values being multiplied by 1000.

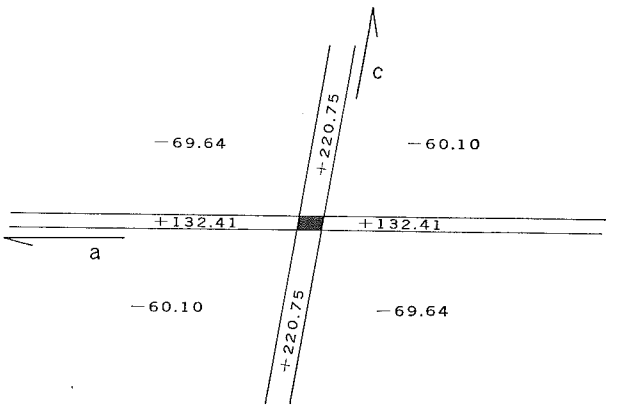

Fig. 3
Allocation of the potential energy of the central ion in the Ca-SO_4 monolayer.

3. Energies of ions adsorbed on various sites of the infinite Ca-SO_4 *monolayer*

Let us consider a Ca-SO_4 monolayer that has an enough wide but definite extension, and suppose that this monolayer is enclosed by boundaries which are parallel only to the a- and c-axis, and also that each of these boundaries has an extension long enough to avoid any energetical interactions from adjacent topographies to reach a major part of each boundary. A such defined monolayer is shown in Fig. 4. To evaluate energies of ions at various sites of this monolayer is a matter of simple mathematics. For instance, the energy of the ion attatched on somewhere in the middle part of the (001) boundary, U_1, can be given by subtracting the interactions of the $+Y_0$ chain (the 0-column), the $+X_0$ and $-X_0$ chains (the 0- and $\bar{0}$-rank), and of the first and second quadrants from the entire energy of the central ion, 446.84, as: $U_1 = 446.84 - 220.75 - 2\times 132.41 - (-60.10) - (-69.64) = 91.01$. Also for an ion on the (100) boundary, the energy is found to be $U_2 = 446.84 - 2\times$

220.75–132.41–(–60.10)–(–69.64)=2.67. The energies of ions at other important sites are also shown in Fig. 4.

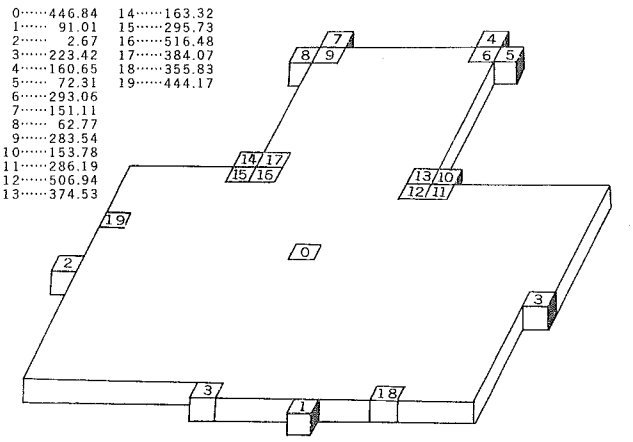

Fig. 4
A model shape of the Ca-SO_4 monolayer and energies of ions at various sites of it.

Now, if the monolayer shown in Fig. 4 is so placed on the (010) surface of a gypsum crystal which has a sufficiently large extension in comparison with the overlying monolayer that there is the exact structural concordance between the two bodies, the boundaries of the monolayer come to form the steps of the mono-atomic height as shown in Fig. 5. At this position of the Ca-SO_4 monolayer, the energies of the ions in this layer gain some additional contributions from all ions and water molecules in the underlying gypsum body. However, since the amount of the new interaction from the underlying gypsum is obviously the same for all ions in the monolayer, the energy values given in Fig. 4 can be used safely for the purpose of discussing the relative stabilities of ions at various sites of the steps.

The most significant information given from Fig. 4 (and also Fig. 5) may be that the energy of the ion adsorbed on the (100) step is negligibly small; $U_2=2.67$. This fact suggests that the tendency of the (100) step to grow in the a-axis direction is also negligible. The (100) plane in macro-size crystal is one of the most distinct cleavage plane. However, cohesion along this cleavage plane is appreciably strong, and difficult to be attributed wholly to such a small interaction as 2.67. Most probably a large part of this cohesion comes from the ion-dipole bonds between ions in the Ca-SO_4 monolayer and water molecules in the H_2O layers lying on and under the Ca-SO_4 monolayer. These water molecules form the ion-dipole bonds, bridging themselves between Ca and SO_4 ions. It is observed in the process of dehydration of gypsum that gypsum crystals split off easily along the c-axis as the

dehydraction proceeds. This fact certainly means that, after water molecules have been dispelled, the ionic interaction alone is not strong enough to keep Ca and SO_4 ions in connection. *Photo* 2 shows the dehydration cracks in dehydrated gypsum.

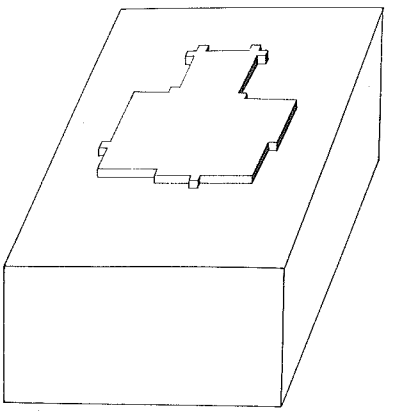

Fig. 5
Superposition of the Ca-SO_4 monolayer of Fig. 4 on the (010) surface of a large gypsum body. The lateral sides of the monolayer come to form the steps of monoatomic height.

4. Stabilities of some important steps

As far as the steps of the monoatomic height is concerned, the step of the most easy occurrence seems to be the (100) step, and the second one the (001). The energies* of ions in the Ca-SO_4 monolayer in the neighbourhoods of these two steps are shown in Figs. 6a and 6b. As seen in these figures, ions in the neighbourhoods of these steps have energies that are more or less deviated from the energy value of the central ion of the monolayer, 446.84. In this regard, the *surface zone* of a given step, or the *marginal zone* of a given boundary in the same meaning, may be difined as the zone where energy values of ions shows some deviations from 446.84. If the total loss of energy in the surface zone of a step is large, the step is not stable. In the case of the (001) step, for instance, the surface zone reaches the four-atom depth and the total energy loss in this zone is found to be 81.39 per the unit length along the a-axis** (5.235 Å). For the (100) step, the surface zone reaches the one-atom depth and the total energy loss is only 2.67 per the unit length along the c-axis** (3.14 Å). Therefore, the (100) monoatomic step is more

* To be exact, the contribution (α) from the underlying gypsum body must be added to all energy values in Figs. 6a and 6b. However, the amount of this contribution is equal for all ions in the monolayer, and hence can be neglected.

** It does not need to mention about the dimension along the b-axis, since it is always equal to the thickness of the Ca-SO_4 monolayer for the surfaces of all monoatomic steps.

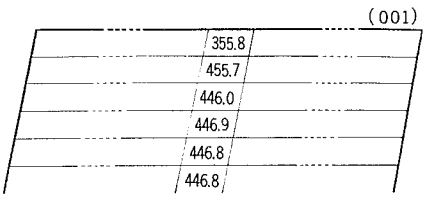

Fig. 6a
Energies of the ions in the neighbourhood of the (001) margin of the Ca-SO_4 monolayer.

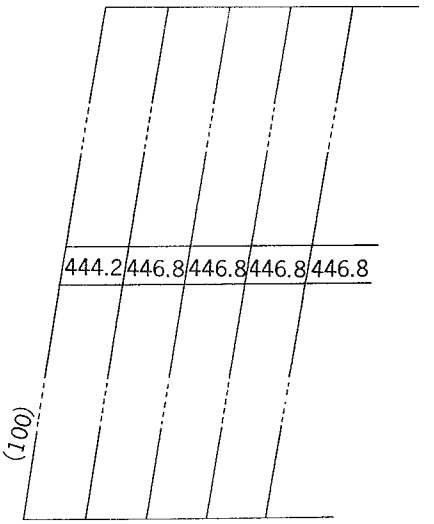

Fig. 6b
Energies of the ions in the neighbourhood of the (100) margin of the Ca-SO_4 monolayer.

stable and easy to occur than the (001) monoatomic step, or in other words, the Ca-SO_4 mono-atomic layer can be split more easily along the (100) plane than the (001). Here (and also hereafter), we are concerned mostlyw ith the stabilities of surfaces of the monoatomic steps which are lateral sections of the Ca-SO_4 monoatomic layer. Since the extension of such a surface in the b-axis direction is confined to the thickness of the monolayer, the surface of this kind may be regarded as "one dimentional surface ". We examine the stabilities of such one-dimentional surfaces because a close relation of them with the stabilities of the corresponding macro surfaces is expected.

As mentioned already in the introduction, the fine steps observed on the cleaved (010) surface are mostly the $(\bar{1}01)$ step, and growth generally takes place on this step. Therefore, to make the nature of the $(\bar{1}01)$ step clear is one of the

primary tasks of the present study. Considering the atomic arrangement of the (010) plane, we hardly assume that the surface of the ($\bar{1}01$) step is a plane of smooth atomic net. The surface may, most probably, consist of the two most stable planes; the (100) and the (001).

On the basis of the above assumption, energy calculations and electron-microscopic observations of the sample were carried out to find what combination of of the (100) and the (001) facets is energetically most possible to form the ($\bar{1}01$) stepped surface. This attempt does not seem completed yet, since there are innumarable combinations which produce anyway ($\bar{1}01$) stepped surfaces. However, energy calculations for a variety of imaginable combinations of the (100) and (001) could give a fairly reliable picture of the real ($\bar{1}01$) stepped surface.

There are many combinations in which one or more ions in the surface zone have energies of negative value, receiving the repulsive interactions. A combination containing ions with negative energies is thought impossible to persist, since such ions are unstable and can not any longer be settled in their own positions. The simplest combination of the (100) and the (001) facets, that is the alternating combination of the (100) and (001) facets of the unit length (5.235 and 3.14 Å) presents an example of this case. As seen in Fig. 7, all ions forming the angles of this stepped surface are of the same sign, and they receive the repulsive interactions of not convergent type from the three diagonal directions; [101], [10$\bar{1}$], and [$\bar{1}$0$\bar{1}$]. The exact estimation of the energy of this angle-forming ion can be done simply by 180° rotation of the hatched portion of the monolayer shown in Fig. 8 around the rotation axis perpendicular to the monolayer at the position of a given angle-forming ion, so as to bring the hatched portion to the crystallographically equivalent position in the opposite quadrant.

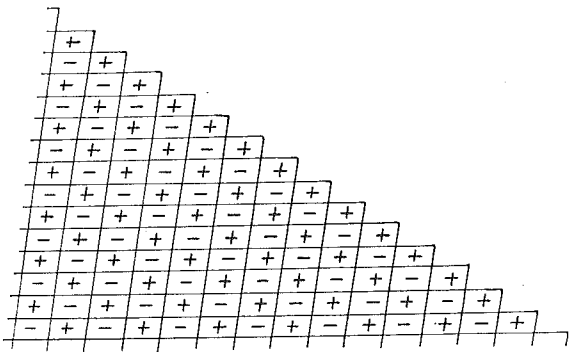

Fig. 7
The simplest combination of the (100) and (001), that is the $1\times(100)-1\times(001)$ stepped plane, and the distributions of the positive and negative ions in it.

Now, as shown in Fig. 8, the angle-forming ion of the original monolayer came to occupy the so-called half crystal position of the new monolayer, while the energy of the ion has been kept unchanged after this rotation operation. If the new monolayer is perfect, the energy of the given ion must be just the half of that of the central ion. However, as seen in Fig. 8, every lattice point along the [101] of the new monolayer is filled with two ions of the same kind, the sign of them being the same as that of the given ion (the ion at the rotation center). In Fig. 8 these overlapping lattice points are shown black. The interactions to the given ion from the extra ions in these overlapping lattice points are summed up to be $\sum_{i=1}^{\infty}(-1000/5.6693i)$, i=1,2,3,....., where the value 5.6693 corresponds to the unit length along the [101] direction. The energy of the given ion is then given as $223.42+\alpha+\sum(-1000/5.6693i)$. The value $223.42+\alpha$ in this equation is the energy value for the ion at the half crystal position of the perfect monolayer, where α is the interaction from the underlaying gypsum unit and thought to be a very small amount. Obviously, the energy of the angle-forming ion of the proposed stepped surface, viz. the combination of the unit (100) and (001), contains as a large part the repulsive interaction of not convergent type, $\sum(-1000/5.6693i)$, which increases with the extension of the stepped surface. The ion, therefore, will become unstable if the stepped surface extends to the [101] direction beyond a distance of a few times of the unit length.

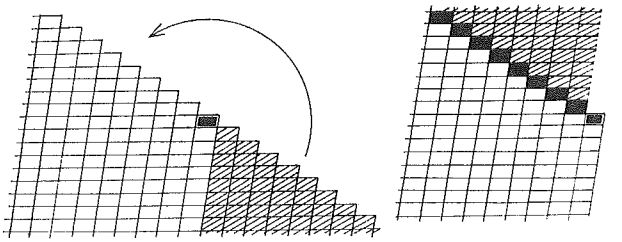

Fig. 8
Rotation-operation applied to the $1\times(100)-1\times(001)$ stepped plane of Fig. 7.

The combination of 3(100)–3(001), in which the (100) and the (001) facets respectively have the extensions of three times of their unit lengths, and similar combinations such as 5(100)–5(001), 7(100)–7(001), and so on, are also unlikely to persist because of unstabilities of the ions forming the angle-tops of these stepped surfaces, although the repulsive interactions along [101] direction are not so rapidly increased with extension as was the case of the 1(100)–1(001) combination. The result of the rotation-operation applied to the 3(100)–3(001) combination, for example, is shown in Fig. 9. In this figure, overlapping lattice points and

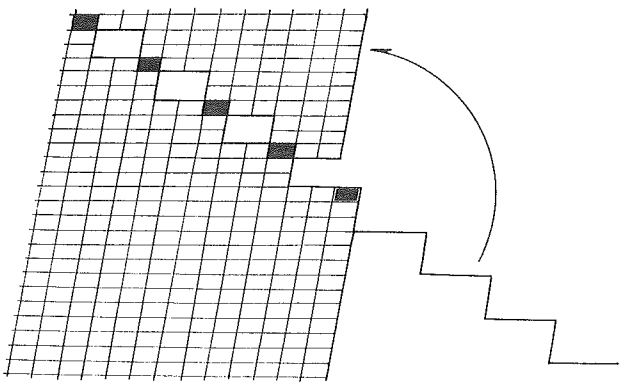

Fig. 9
Rotation-operation of the 3(100)−3(001) stepped plane, which yields a sequence of alternating vacancies and overlapping lattice points.

vacancies are seen to appear alternatingly along the [101] direction. Each vacancy occupies adjoining four atom positions, and the overlapping lattice points distribute by a distance of 11.3384i (Å) from the ion at the half crystal position. The total interaction of all overlapping ions to the given ion (the ion at the angle-top of the 3–3 combination) therefore is $\sum(-1000/11.3384i)$, $i=1,2,3,\ldots\ldots$ This repulsive interaction increase infinitely as the plane extends to the [101] direction. Here, it is of convenience to define the *interaction from a vacancy* as the negative of the imaginary interaction that would be yielded if the vacancy is occupied properly by atoms. For instance, the first vacancy of Fig. 9 occupies the four atom positions, (−1, 1), (−1, 2), (−2, 1) and (−2, 2). If these four positions are actually filled with proper atoms, the total interaction from these four ions to the ion at the half crystal position must be $-176.398+132.926+95.681-88.195=-35.977$. Thus, the interaction of this vacancy is $-(-35.977)=+35.977$*.

When a vacancy occupies atom-positions of an even number, the electrostatic interaction from the vacancy to a given ion decreases very rapidly with distance. This is because the vacancy of an even atom-position acts like the neutral field to a distant ion owing to the compensation of the positive and negative ions of the same number. In the case of the 3(100)–3(001) stepped plane, for example, the first vacancy of Fig. 9 yields the interaction of +35.977 to the ion at the rotation center. And those from the second, third, and fourth vacancy show a very rapid decrease with distance as: +1.190, +0.255, and +0.093 respectively. Therefore, the angle-forming ion of the 3(100)–3(001) becomes increasingly less stable with the extension of the plane, since the positive interactions from the vacancies converge

* $A-(-35.977)=A+35.977$, where A is the energy of the ion at the half crystal position of the perfect monolayer, that is $223.42+\alpha$.

to zero much more quickly than the negative interactions from the overlapping lattice points do.

The unstability of the ion forming the angle-top is an inevitable feature of the all combinations of n(100)–n(001) type, where n is an odd number, since they always contain vacancies occupying atom-positions of an even number, and have the repulsive interaction of not convergent type along the [101]. The same feature may also be seen in most of the n(100)–n(001)–m(100)–m(001) combination where n is an odd, and m is an even number.

There are, on the other hand, many combinations where all ions have some positive energies and are, at any rate, stable in the combinations. Among them are all combinations of m(100)–m(001) type where m is an even number, and some complicated combinations of the n(100)–m(001)–n(100)–m(001)–m(100)–n(001)–m(100)–n(001) type. As an example of the last case, a fairly stable combination is obtained when m=2 and n=3. The energies of all surface ions of this combination is shown in Fig. 10. The calculations of these energies required a tedious work to apply the rotation-operation to every ion on the surface so as to obtain any geometrical patterns of the distributions of vacancies and overlapping lattice points.

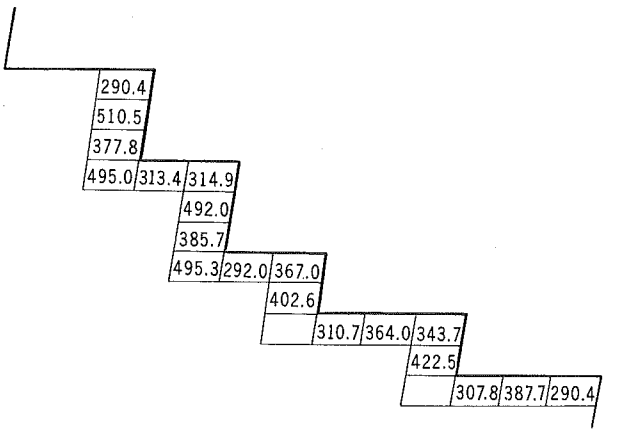

Fig. 10
Energies of the ions forming the surface of the 3(100)−2(001)−3(100) −2(001)−2(100)−3(001)−2(100)−3(001) monoatomic stepped plane.

All energetically possible combinations, in which all constituent ions have positive energies, may be expected to exist at any rate in the real ($\bar{1}01$) plane, though their frequencies of appearance may be different according to the stabilities of these combinations. Farther, even the combinations of the n(100)–n(001) type, in which the angle-forming ions come to have negative energies when the extensions of the planes are beyond some limits, may have chances to appear in the real ($\bar{1}01$)

plane, composing a part of it of some limited extension. Electron-microscopic observation on the ($\bar{1}01$) cleaved step on the sample seems to indicate the possibility that the real ($\bar{1}01$) plane is composed of not a single combination but a complex of two or more different combinations. As shown in *Photo* 3, the ($\bar{1}01$) step lines under electron-microscope are not always straight, but in places consist of gentle curvatures, nevertheless keeping the general orientation of ($\bar{1}01$) as a whole. Occasional angular rises on the step lines are also observed. This rise may correspond to the solid angle consisting of the (100) and (001) faces of very long extensions, which may be denoted as ∞(100)–∞(001). It seems that these rises take position between two different combinations and act as a buffer between the two combinations.

Two models of the combination were finally chosen as highly possible. These are the combination of 2(100)–2(001) with a more or less periodical distribution of the ∞(100)–∞(001) rises as shown in Fig. 11, and the 3(100)–2(001)–3(100)–2(001)–2(100)–3(001)–2(100)–3(001) combination also with the ∞(100)–∞(001) rises distributed in it by a distance of sufficiently long. Probably, the real ($\bar{1}01$) stepped plane may composed of a complex of these two models. The energy calculation for the 2(100)–2(001) combination was made in some detail. The energies of the ions in the surface zone were calculated to the five-atom depth and are shown in Fig. 12. In fact the surface zone of the 2(100)–2(001) combination seems to reach considerably deep. Although the exact estimation of the depth has not yet been done, there is a certain indication that the energy of the ion at the 20-atom depth still deviates appreciably from the energy value of the central ion. The total energy loss of the surface zone, however, was found obtainable with a good accuracy by an empirical method, without knowing of the exact value of the

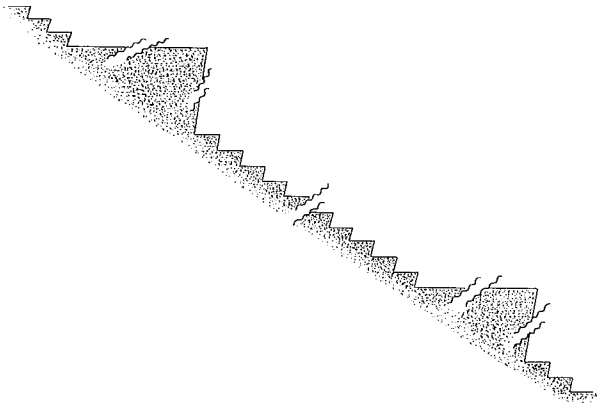

Fig. 11
A model of the ($\bar{1}01$) stepped plane; the combinations of the 2(100)–2(001) and the ∞(100)–∞(001).

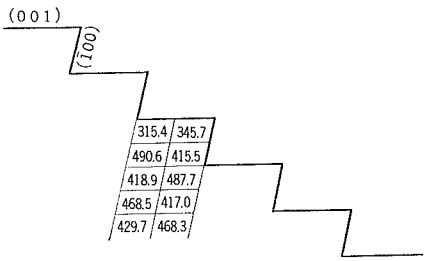

Fig. 12
Energies of the ions in the surface zone of the 2(100)−2(001) stepped plane.

depth of the surface zone. The total energy loss thus found was 215.9/(10.47+6.28 Å). This value indicates that the 2(100)–(001) combination is highly stable.

In the neighbourhood of the ∞(100)–∞(001) rise, the energies of the ions in the surface zone of the 2(100)–2(001) come to be more or less modified, being affected by the interaction from the rise. These energy changes are shown in Figs. 13a. and 13b. The amounts of the changes are not large, and suggest that the addition of the ∞(100)–∞(001) rise to a combination does not modify the energy configuration of the original combination much, and also that an essential role of the rise may be to absorb the interaction between two different combinations, between which the rise is apt to appear, to make them more stable.

Energy calculations for the other model, that is the 3(100)–2(001)–3(100)–2(001)–2(100)–3(001)–2(100)–3(001) have not been completed yet, and this model

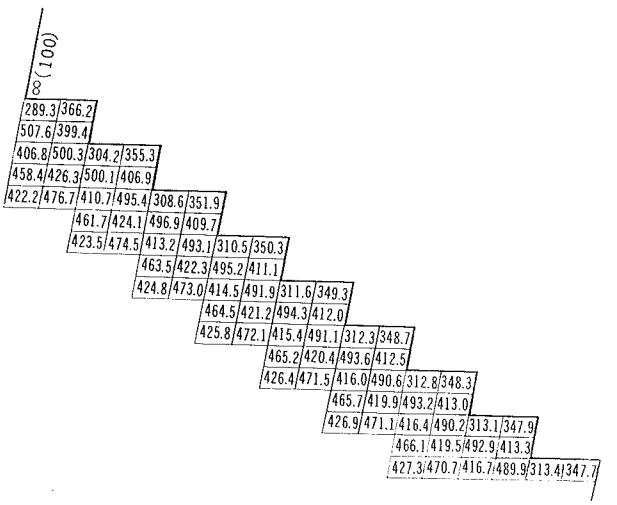

Fig. 13a
Energies of the ions in the surface zone of the 2(100)−2(001) plane in the neighbourhood of the ∞(100) cliff.

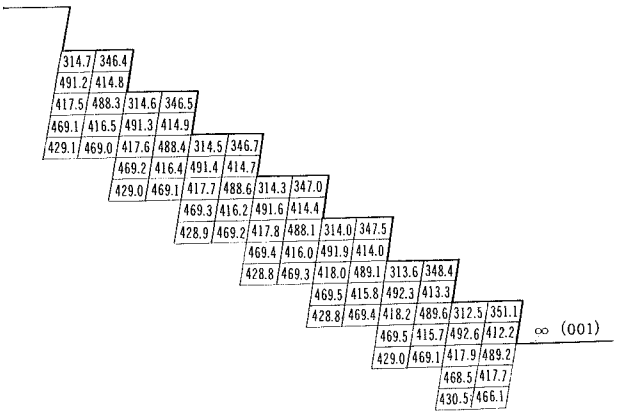

Fig. 13b
Energies of the ions in the surface zone of the 2(100)–2(001) plane in the neighbourhood of the ∞(001) plane.

will not be used for the further discussion. However, the surface of this combination is highly stable as shown in Fig. 10, and hence there is only a little possibility that the part of this combination as well as the part of the 2(100)–2(001) combination provides with very active sites for the growth of the stepped plane.

5. Growth sequence on the ∞(100)–∞(001) rise

The energies released or required when an ion is adsorbed on various sites were calculated for all possible sites on the surface of one of the proposed models, that is the 2(100)–2(001) with distributions of the ∞(100)–∞(001) rises in it. The result is shown in Fig. 14. As seen in the figure, the most active site through the whole surface of this model is the site on the edge of the rise (the rise-edge hereafter), where an energy of 160.65 is released if an ion is adsorbed. At a very slow rate of growth, therefore, the first adsorbed ion is expected to come and settle in this

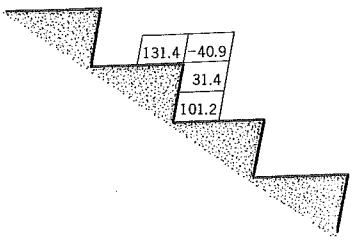

Fig. 14-a
Energies released or required when an ion is adsorbed on various sites of the surface of the 2(100)-2(001).

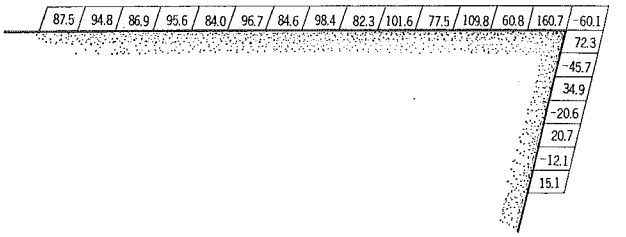

Fig. 14-b
Energies released or required when an ion is adsorbed on various sites of the surface of the ∞(100)-∞(001) rise.

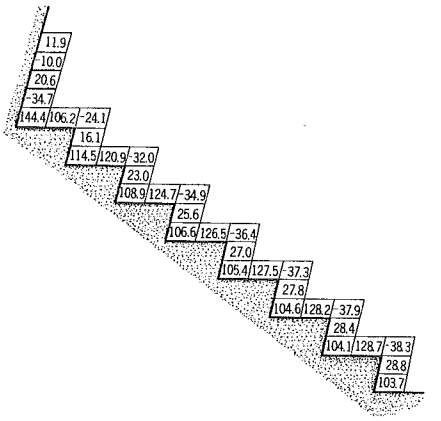

Fig. 14-c
Energies released or required when an ion is adsorbed on various sites of the 2(100)-2(001) surface in the neighbourhood of the ∞(100) cliff.

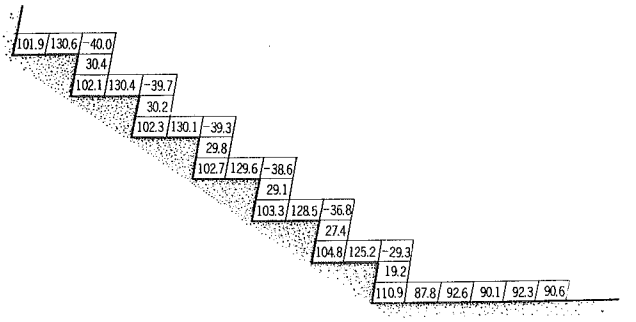

Fig. 14-d
Energies released or required when an ion is adsorbed on various sites of the 2(100)-2(001) surface in the neighbourhood of the ∞(001) plane.

position in preference to other sites of lesser active. If an ion is adsorbed on a site, the enery configuration in the neighbourhood of the site is completely changed, and new calculations have to be made to find out the most active site for the next coming ion. The sequence of adsorptions of ions obtained by such calculations is shown in Fig. 15.

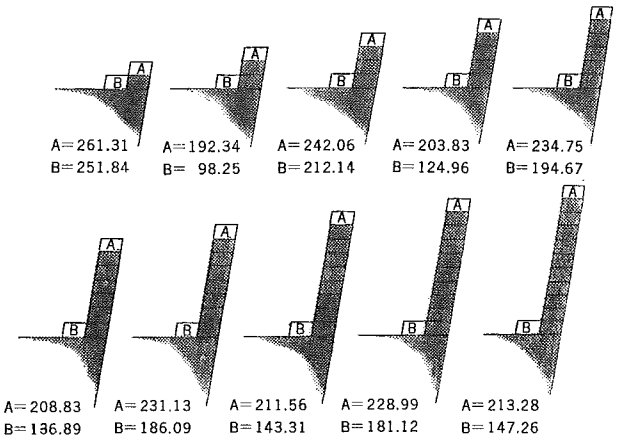

Fig. 15
The sequence of adsorption of ions on the site of the edge of the ∞(100)–∞(001) rise.

As immediately seen in Fig. 15, the most characteristic feature of the growth sequence on the ∞(100)–∞(001) rise is that, after the site of the rise-edge is occupied by the first ion, the second ion comes not to the kink position formed on the left side of the first adsorbed ion but to the position of being piled up on the first ion in the c-axis direction. So does the same the third, fourth, fifth ion and so on, a single atomic Ca-SO_4 chain starting from the edge of the rise and running in the c-axis direction is finally made up. At an early stage of the growth of this chain, the energy of the ion on the top of the chain fluctuates greatly. However, as the growth proceeds and the chain has attained a certain length that is enough to avoid the interaction from the rise (from which the chain started to grow) to reach the top of the chain, the energy of the top ion comes to settle in a value of 220.75. This value is nearly equal to the energy of the ion adsorbed on the kink of the half crystal position (=223.42), and indicates a very high growth rate of the chain at this stage.

After the first chain thus formed has attained a certain length, the second chain will start to grow from the kink position formed on the ground of rise at the root of the first chain, and elongates itself also in the c-axis direction, keeping the contact with the first chain. In this case, it may be a problem to define when the

chance be bestowed for the second chain to start to grow. It may largely depend on the degree of supersaturation of the solution, and also to some extent on the mobilities of ions in the solution. The authors' opinion on this problem is as follows:

a) If two or more growth sites are separated from each other by not long distances and hence there are appreciable electrostatic interactions among them, the activities to adsorb an ion of these sites vary every moment as one of them adsorbs an ion. This means that the growths of these sites are carried on under an influence of their mutual interference. We call such a growth process *controlled growth for a given set of growth sites*. If several sites are in the state of controlled growth at an extremely slow rate, that is to say the quasi-equilibrium rate, there may by scrambles for available ions among these sites, or even flows of ions from less active sites to the most active one. The growth sequence in this case is simply to follow the most active sites at every moment perfectly, without any mistake of lesser active sites for the most active one. We call this unequivocal process the *ideal course for a controlled growth.*

b) If a controlled growth is carried on at a practical rate, there may be cases that an ion is adsorbed rather on a less active site than on the most active one by accident. Such an accidental adsorption is sometime merely a detour which gives the ideal course a few steps back, but in some cases it makes the growth sequence greatly deviated from the ideal course. The probability of an accidental adsorption to happen increases as the growth rate increases, and also when there are not much differences in the energies of given sites, and when these sites are separated from each other by comparatively long distances. An imaginable deviation from the ideal course may be defined as " highly probable ", " little probable ", or " improbable ", by taking the above mentioned factors into consideration.

c) If growth sites are separated from each other by enough distances to avoid appreciable interactions among them, they can grow independently with their own growth rates that are proportional to their activities. The growth process of this kind may be called *independent growth.*

According to the criterion discussed above, the time of the second chain to start to grow is defined to be after the first chain has attained a certain length that is enough long to avoid a greater part of the interaction from the rise to reach the top of the chain, provided that the growth process proceeds at a very slow rate. The growth sequence of the second chain is exactly the same as that of the first chain. That is, the probability of an ion to be adsorbed on the top of the second chain is always a more higher than that of an ion to be adsorbed on the kink position formed at the root of the chain. If compared with the corresponding values of the first chain, however, the energies of the top-ions at every moment of growth of the second chain are found to be increased with a very few addition of 2.66, which is just the amount of the lateral interaction from the single $Ca\text{-}SO_4$ chain of the in-

finite length; it is obvious that we can convert the first chain to the position of the second chain by bringing a Ca-SO_4 single chain of the infinite length into contact with the first chain on its right side.

The same sequence of growth as described above can be applied to the growth of the third, fourth, fifth chain and so on, and in consequence there appears a band of single Ca-SO_4 chains which are in contact side by side and running in the c-axis direction with almost equal speeds. The tops of these chains have been handicapped from the beginning so that they keep a certain distance to/from their immediate neighbours. This distance between neighbouring two tops is, as mentioned above, considered to be enough long to avoid the greater part of the interference between the two tops. Therefore, every chain at this state can grow independently, without any appreciable interferences from nearby topographies. In such a state, the energy released when an ion is adsorbed on the top is 220.75 for the first chain, and 223.41 for other chains. These high values indicate that these tops are very active to adsorb ions, and that their growth rates are comparable to the growth rate of the most active kink available in the gypsum crystal (=223.42).

Photo 1 shows a very early stage of the growth on the (010) cleaved surface. There are many fine needles starting from the ($\bar{1}$01) step and running in the c-axis direction. The left-hand side (facing the photo) of each needle forms a very accute termination toward the top. To this termination side, any reasonable facial index can not be given. This fact is thought to be a good evidence of the independent growth of such a kind as described above. It should be mentioned in this regard that the growth pattern shown in *photo 1* can be observed very commonly even in the growth processes at comparatively high growth rates. The attainment of the independent growth may be not so difficult for a band of the Ca-SO_4 chains in the beginning stage of growth.

At the stage of this independent growth of every chain, the fact that the activity to adsorb an ion of the top of the first chain is always a little weaker than the activities of the tops of the following chains is of a not little significant. This fact means that the first chain will sooner or later be caught up by the second chain. Generally speaking, if a chain is approached by its immediate follower, the tops of the both chains come to grow under an influence of the mutual interference between them, and this makes the growths of the both chains retarded. Consequently, the tops of all other chains following the retarded two can approach them, and then all chain-tops in a band begin stand in line, forming a flat surface which has a reasonable facial index. If a band has attained this stage, no chain in the band can grow independently, being free from interferences from other chains. This is the stage of the controlled growth for a band of chains.

It is not the scope of the present paper to deal with a full examination of the controlled growth for every possible case. Several examples of rather simple

cases are given. A series of special notations is used for describing a set of growth sites for which the controlled growth is to be examined. The first chain in a band is denoted A, the second chain B, and the third, fourth, fifth chain and so on C, D, E, and so on. A notation $A_2B_5C_3D_{12}E$, for example, denotes a band consisting of the five chains from the first to the fifth, in which the top of the first chain is ahead to that of the second chain by the two-atom distance, the top of the second chain to that of the third by five atoms, the third to the fourth by three, and the fourth to the fifth by twelve atoms. The energy released or required when an ion is adsorbed on the top of the first chain of this topography is specified by a notation A: $(A_2B_5C_3D_{12}E)$. Similarly, the energies on the top of the second, third chain so on by B: $(A_2B_5C_3D_{12}E)$, C: $(A_2B_5C_3D_{12}E)$ and etc.

Now consider the simplest case of the controlled growth that two chains in immediate contact grow under electrostatic interference to each other. Shown in Table 4 are the changes of the activities of the tops of the two chains as the distance between the two tops is diminished. Although there are considerable fluctuations from moment to moment of both activities, it is seen that the top of the second chain is always more active than the top of the first chain until the dis-

Table 4. Energies of ions adsorbed on A_nB.

	A : (A_nB)	B : (A_nB)
$n=\infty$	220.75	223.41
.....	.....	.....
n=20	213.10	215.39
19	228.77	231.86
18	212.30	214.49
17	229.67	232.86
16	211.30	213.37
15	230.79	234.12
14	210.04	211.94
13	232.22	235.77
12	208.39	210.02
11	234.14	238.01
10	206.15	207.36
9	236.80	241.22
8	202.94	203.41
7	240.75	246.19
6	*197.97	*196.99
5	247.17	254.77
4	*189.39	*185.04
3	259.12	272.24
2	*171.39	*158.35
1	285.81	311.94
0	*132.81	*120.92

* A : (A_nB) is larger than B : (A_nB) here.

tance becomes the six-atom length. That is, the top of the second chain constantly gets close to the top of the first chain until they come to form the topography A_6B. As for the topography A_6B thus formed, however, the activity relation between the two tops is found reversed for the first time, and hence, the topography A_6B must be turned back to A_7B in the next step of growth. Therefore, if there are no other chains which interfere the two chains, the ideal course for the controlled growth of the two chains is the repeated steps of $A_6B-A_7B-A_6B-A_7B-A_6B-$.

When the two chains continue to grow by repeating the A_6B and A_7B steps, the growth rate is determined by the frequency with which an ion is adsorbed on the top of the first chain of the topography A_6B to form the A_7B. That is, the growth rate of the process $A_6B—A_7B—A_6B—A_7B—$ is determined by the value of A: (A_6B) and not by B: (A_7B), because A: (A_6B) is smaller than B: (A_7B). Therefore, while the first and second chains are continuing to grow by this process with the rate proportional to 196.99, the third chain approaches them with a higher speed that is proportional to 223.41. The controlled growth of the three chains begins when the tops of the preceding two chains came into the reach of an appreciable interaction of the approaching third chain. The feature of the changes of the energies on the tops of the three chains in controlled growth is shown in Table 5.

As seen in Table 5, the top of the last coming chain (the third chain) is always

Table 5. Energies of ions adsorbed on A_6B_nC.

	A : (A_6B_nC)	B : (A_6B_nC)	C : (A_6B_nC)
$n=\infty$	197.97	196.99	223.41
.....	.....	.....	.....
n=24	203.07	190.57	222.00
23	192.70	203.67	224.94
22	203.42	190.01	221.76
21	192.33	204.28	225.16
20	203.82	189.34	221.46
19	191.90	205.01	225.55
18	204.28	188.54	221.06
17	191.40	205.91	226.02
16	204.81	187.54	220.52
15	190.82	207.03	226.64
14	205.45	186.28	219.79
13	190.12	208.46	227.53
12	206.21	184.63	218.71
11	189.28	210.38	228.83
10	207.15	182.39	217.09
9	188.24	213.04	230.88
8	208.31	179.18	214.46
7	186.92	216.99	234.35
6	*209.81	174.21	*209.75

* A : (A_6B_nC) is larger than C : (A_6B_nC) here

more active than the tops of the first and second chains until they form the topography A_6B_6C. The same is said of the controlled growths starting with the topographies $A_6B_6C_nD$, $A_6B_6C_6D_nE$, and so on. The last chains of these topographies are always more active than the preceding chains and therefore approach to them until $A_6B_6C_6D$, $A_6B_6C_6D_6E$, and so on, are formed. These features are seen in Tables 6 and 7.

The growth processes described above are the ideal courses for the controlled growths of two, three, four, and five chains, and it is obvious that they were produced with a more or less artificial setting of growth course. That is, the tops of the preceding chains which already have formed the topographies A, A_6B, A_6B_6C, and $A_6B_6C_6D$, respectively, were supposed, according to the definition of the ideal course, not to grow until the tops of the last coming chains arrive at the positions of n=6 and form the topographies A_6B, A_6B_6C, $A_6B_6C_6D$, and $A_6B_6C_6D_6E$, respectively. This setting is not irrational at all, since a topography $A_6B_6C_{i-1}D$, for instance, is always the most probable topography to follow the $A_6B_6C_iD$ for every i of more than seven. One may, nevertheless, think that such an ideal course

Table 6. Energies of ions adsorbed on $A_6B_6C_nD$.

	A : $(A_6B_6C_nD)$	B : $(A_6B_6C_nD)$	C : $(A_6B_6C_nD)$	D : $(A_6B_6C_nD)$
n=∞	209.81	174.21	209.75	223.41
.....	.....	.....	.....	.....
n=15	215.35	167.06	219.79	232.38
14	204.06	181.69	199.04	213.84
13	215.76	166.36	221.22	233.71
12	203.63	182.45	197.39	212.29
11	216.23	165.52	223.14	235.52
10	203.12	183.39	195.15	210.12
9	216.78	164.48	225.80	238.17
8	202.52	184.55	191.94	206.84
7	217.43	163.16	229.75	242.35
6	*201.81	186.05	186.97	*201.35

Table 7. Energies of ions adsorbed on $A_6B_6C_6D_nE$.

	A :	B :	C :	D :	E :
n=∞	201.81	186.05	186.97	201.35	223.41
.....	.....	.....	.....	.....	.....
n=12	206.75	179.87	195.21	188.99	217.19
11	196.71	192.47	178.28	214.74	230.26
10	207.07	179.36	196.15	186.75	215.55
9	196.39	193.02	177.24	217.40	232.55
8	207.43	178.76	197.31	183.54	212.66
7	195.99	193.67	175.92	221.35	236.31
6	*207.85	178.05	198.81	178.57	*207.61

could hardly be held in a growth process carrying on at a practical rate. In fact, however, we can observe rather commonly the linear pattern of growth which corresponds to the configuration $A_6B_6C_6D_6E_6F_6\ldots\ldots$, on the terminating side of the needles grown at not very slow growth rate. Probably, the degree of supersaturation changes sensitively according to the density of active growth sites so as to make up a circumstance where some growth sites whose activities are lower than a critical value can not grow effectively.

If the growth attained a stage where there are no more chains coming after the preceding chains which already have formed a topography $A_6B_6C_6D_6E_6\ldots\ldots$, and then the supersaturation is restorred for these less active sites, the growth will restart from one of these sites. Energy calculations show that the growth in this stage always starts from the top of the first chain, and furthermore that after regaining its growth the top of the first chain is always more active to adsorb an ion than the other chains. Thus, the topography $A_6B_6C_6D$, for instance, follows the course $A_7B_6C_6D$—$A_8B_6C_6D$—$A_9B_6C_6D$—for the ideal course until it becomes $A_\infty B_6C_6D$. After the first chain had an enough length, the second chain can start to grow, following the course $A_\infty B_7C_6D$—$A_\infty B_8C_6D$—$A_\infty B_9C_6D$—. The same holds of the third, fourth, fifth chain and so on, there again appears a band of chains growing independently. This may be called *rejuvenation of the independent growth* for the band.

The rejuvenation of the independent growth seems to be a common phenomenon. Many needles of the middle stage of growth show a combined form of a very accute terminating part and a less accute facet on their left side. The accute terminating part corresponds to the part of the independent growth regained, and the facet to the part that is still remained in a configuration of, say, $D_6E_6F_6G_6H_6\ldots\ldots$, to which the facial index (601) is applicable. Fig. 16 illustrates this form of the needle schematically. One may see a great resemblance between this figure and the actual form of the needle shown in *Photo 4*. Data of the energy calculations indicating the rejuvenation of independent growth are shown in brief in Table 8.

All examples which have been described above are those of the ideal courses for some controlled growths. However, there may be often a case that the growth course is deviated from the ideal one by accidental adsorptions of ions on less active sites. As for the controlled growth of two chains, the ideal course A_6B—A_7B—A_6B—A_7B—may sometime be broken by the adsorption of an ion on the less active top, viz. the top of the second chain, to form A_5B, and then A_4B. This deviation is highly probable because there is only a little difference between the values of A: (A_6B) and B: (A_6B). The topography A_4B thus formed is another barrier* to prevent the top of the second chain to approach nearer the top of the

* The topography A_6B provides the first barrier.

Table 8. Energies of ions adsorbed on A_nB_6C, $A_nB_6C_6D$, and $A_nB_6C_6D_6E$.

	A : (A_nB_6C)	B : (A_nB_6C	C : (A_nB_6C)
n= 6	209.81	174.21	209.75
7	229.70	223.41	185.15
8	213.28	180.63	208.04
9	227.07	218.44	186.65
10	215.33	184.58	206.72

	A : ($A_nB_6C_6D$)	B : ($A_nB_6C_6D$)	C : ($A_nB_6C_6D$)	D : ($A_nB_6C_6D$)
n= 6	201.81	186.05	186.97	201.35
7	237.32	235.25	162.37	217.72
8	205.99	192.41	185.26	202.13
9	234.04	230.22	163.87	217.40
10	208.64	196.36	183.94	203.14

	A : ($A_nB_6C_6D_6E$)	B : ($A_nB_6C_6D_6E$)	C : ($A_nB_6C_6D_6E$)	D : ($A_nB_6C_6D_6E$)	E : ($A_nB_6C_6D_6E$)
n= 6	207.85	178.05	198.81	178.57	207.61
7	231.50	227.25	174.21	194.97	195.31
8	211.61	184.47	197.10	197.35	207.17
9	228.61	222.28	175.71	194.26	195.73
10	213.92	188.42	195.78	180.00	206.78

first chain. Because, for this topography the value A: (A_4B) is considerably larger than B: (A_4B), and the two tops are situated more close together than those in the A_6B. Therefore, the possibility that an ion is adsorbed on the top of the second chain to form A_3B is certainly not high. The occurrence of the growth process A_4B—A_5B—A_4B—A_5B—is therefore highly probable, and, if once occurred, would last more persistently than the process A_6B—A_7B—A_6B—A_7B—.

Similarly, the topographies A_2B and A_0B provide the third and the fourth barriers to prevent the second chain to reach and overtake the first chain. These two barriers are higher than the A_6B and A_4B, and there may be almost no possibility for the second chain to overtake the first chain. The processes A_2B—A_3B—A_2B—A_3B—and A_0B—A_1B—A_0B—A_1B—may therefore be very persistent.

Just as the topography A_6B leads to form the configuration $A_6B_6C_6D_6E_6\ldots$, the topographies A_4B, A_2B, and A_0B produce the $A_4B_4C_4D_4E_4\ldots\ldots$, $A_2B_2C_2D_2E_2\ldots\ldots$, and $A_0B_0C_0D_0E_0\ldots\ldots$, respectively, which correspond to the facets (401), (201), and (001). Although these facets, especially the (201) and (001), are very stable and very persistent, the independent growths may still be regained in the same way as for the (601), if there are no other sites approaching them with a higher growth rate. Energy data are given in Tables 9 and 10 for the case of the formation of $A_2B_2C_2D$ and its rejuvenation.

An interesting fact is that almost all linear patterns that we can observe on the sample are only those to which the facial indices (101) and (601) are applicable.

Table 9. Energies of ions adsorbed on $A_2B_2C_nD$.

	A:	B:	C:	D:
n=∞	198.35	109.52	188.88	223.41
.....	.....	.....	.....	.....
n=10	188.44	121.36	174.28	209.41
9	208.88	96.76	204.93	238.63
8	187.12	123.34	171.07	206.46
7	210.37	94.45	208.88	242.57
6	185.43	126.06	166.10	201.37
5	212.29	91.20	215.30	249.43
4	183.22	129.99	157.52	191.68
3	214.84	86.39	227.25	263.89
2	*180.28	135.94	140.05	*168.99

Table 10. Energies of ions adsorbed on $A_nB_2C_2D$.

	A:	B:	C:	D:
n=2	180.28	135.94	140.05	168.99
3	252.48	249.83	83.10	206.95
4	194.73	162.63	132.65	172.39
5	242.79	232.36	89.05	204.01
6	201.59	174.58	127.84	174.94

In fact, we could find only one face to which a facial index other than (101) and (601) was given; that was (401). The fact that the (601) face is commonly observed on the sample indicates that the ideal course leading to the formation of the configuration $A_6B_6C_6D_6E$..... is not unusual phenomenon even in growths carrying on at practical growth rates. The crystallodynamic nature of the (101) face, on the other hand, remains in some obscurity. This face may possibly be a combination of (100) and (001) which can be denoted as m(100)-m(001), and so stable as comparable to the (001) face.

As for the formation of the (101) face, however, there are certain evidences that it is formed in circumstances where the growth of the first chain in a band is hindered by some reasons. Such a hinderance may inevitably happen whenever the top of the first chain reaches the edge of the sample. Before the chain reaches the edge, it grows, being laid on the (100) surface of the sample and supported with a certain addition, though it may be very small, of the interaction coming from the underlying gypsum body. After has reached the edge, however, the chain has to grow without any support and extend itself into space. This situation makes the growth rate of the first chain slower than when the chain was growing on the (010) surface, and hence gives the late-coming chains chances to approach nearer the top of the first chain to form the (101) face.

Photo 5 shows the case that the first chains of several bands reach the edge of

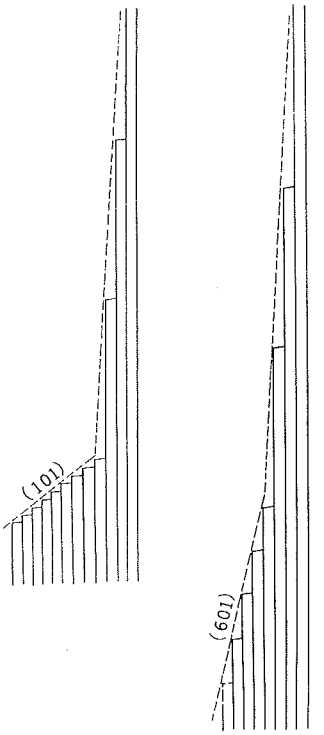

Fig. 16
Two shapes of a band of the Ca-SO_4 single chains, each showing a combination of the independent and controlled growths of the chains.

the sample and the (101) faces are formed there when the late-comers caught up the first chains. In this regard, it is of interest to observe that these (101) faces at the edge form eaves-like overhangs, extending themselves beyond the edge of the sample. The explanation of this phenomenon is, however, not difficult. When reached the edge of the sample, the top of the first chain still maintains the activity of 220.75, and provides the most active site on the edge surface. On the other hand, it is reasonable to suppose that the most active site on the original edge surface may have an energy which is not so much different from the energy value of the most active site on the (101) stepped surface, 160.65, since the edge of the sample and the cleaved step on the sample can generally be produced by the same mechanism. Therefore, it may be an usual case that the growth on the edge surface of the sample does not take place until the tops of the chains have reached the edge and provided there with the very active sites which have the energy value of 220.75. The overhangs are thus formed, starting from these active sites.

It may also be a case that the growth of a chain (not necessarily be only the

first chain) in a band is hindered by other reasons such as the adsorption of a foreign atom on the top or a barricade of certain lattice defect existing on the course of the given chain. In some cases the hindering effect may be so severe that the growth of the hindered chain is actually stopped. The dead chain is then caught up by its followers, and the (101) face is formed. In this case the possibility for the dead chain to regain the independent growth is obviously very little, and the chance for a late-coming chain to overtake the dead chain is also very few due to the high barrier of A_0B. As adjacent bands continue to grow, the dead band with the (101) facet on top is left behind, forming a canal-like narrow depression parallel to the c-axis among the adjacent bands which are still growing actively. *Photo 6* illustrates this canal-like depression. This is also a very common feature on the growing (010) surface of gypsum.

6. Growth sequence on the 2(100)–2(001) part of the step

The energies released or required when an ion is adsorbed on various sites on the surface of the 2(100)–2(001) part of the (101) step were calculated and shown in Fig. 14-a. Through the whole surface of the 2(100)–2(001) part, as seen in this figure, there are no sites more active than the site of the edge of the ∞(100)–∞(001) rise. Therefore, if the degree of supersaturation of the solution is supposed to be so critical that it allows only the most active site on the whole surface of the (101) step, we do not need considering about the growth of the 2(100)–2(001) part any more. In such a case, formations of the single chains, occurring at first on the site of the edge of any ∞(100)–∞(001) rise, will propagate from the right to the left, then go into the territory of the 2(100)–2(001). The width of a band of

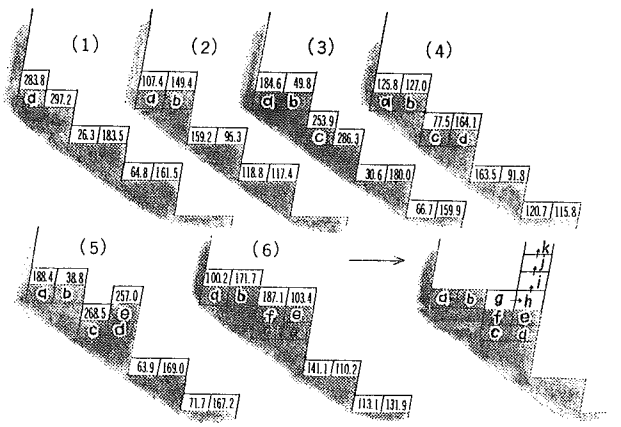

Fig. 17
The sequence of adsorption of ions on the 2(100)-2(001) surface in the neighbourhood of the ∞(100) cliff.

chains in this case corresponds to the distance by which two adjacent rises are separated from each other.

A case like that described above may be possible if the growth is carried on at an extremely slow rate. However, since the 2(100)–2(001) part and the ∞(100)–∞(001) rise are separated from each other by an enough distance to avoid the mutual interaction, the simultaneous initiation of growth at the both parts is also

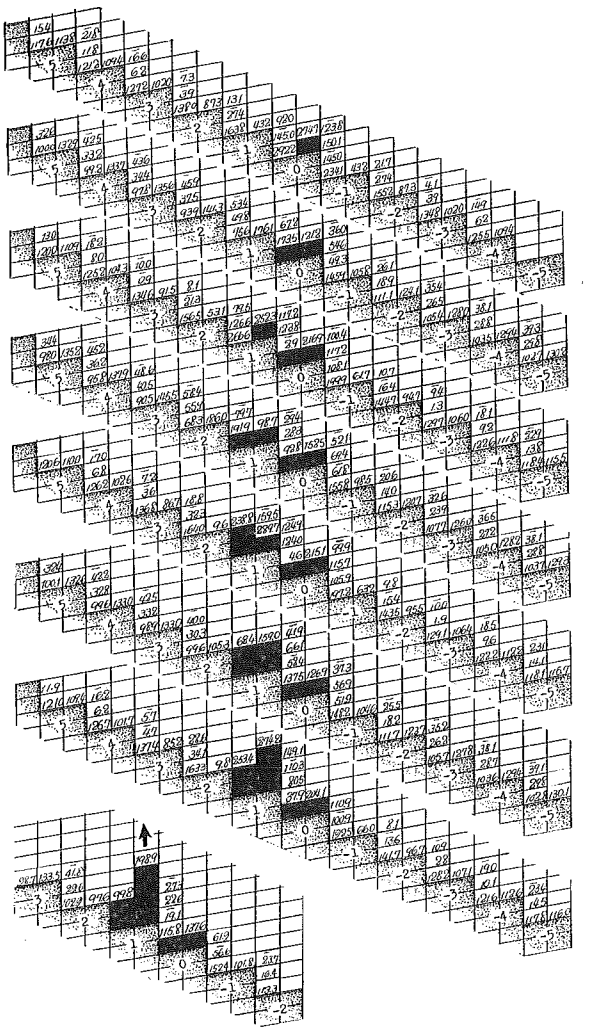

Fig. 18
The most possible sequence of adsorption of ions on the 2(100)-2(001) surface.

highly possible in the growth of practical rates. Two examples of such cases are shown in Figs. 17 and 18. In Fig. 17, the growth is initiated at the kink position formed at the root of the ∞(100) cliff. The energy released when an ion is adsorbed on this site is 144.4, showing that this site is the most active in the 2(100)–2(001) part of the step. The example in Fig. 18 shows the case that the initiation of growth takes place at the most active site in the middle part of the 2(100)–2(001), where the energy of 131.4 is released when an ion is adsorbed.

It is obvious in these figures that the characteristic tendency of growing to the c-axis direction in the form of the single chain appears in both the growing domains, after a few beginning steps of their growth sequences. Careful observations on the grown sample reveal very thin, whisker-like bright lines running parallel to the c-axis, among much wider bands. These lines may be very thin bands of chains of this occurrence.

The examination of possible deviations from the ideal course of growth of this part of the (101) step is very difficult, since during the growth process there often appear several or more sites which are nearly equal in activity. A generalization, however, may be given as follows:

The growth process actually prevailing in the field of the 2(100)–2(001) part may be a complex one, composed of three major processes, that is, the process of growing to the c-axis direction in the form of the single chain as described in Figs. 17 and 18, the process of forming a x(100)–x(001) rise where x is some large number, and the process of advancing the 2(100)–2(001) stepped surface, keeping its configuration unchanged.

7. *Remarks on the growth of seed crystal*

As a necessary course of this study, the growth of a seed crystal was carried out. The seed crystal was a tabular cleavage fragment parallel to the (010), and had the initial weight of 199.3 mg., the surface area of 127 mm^2, and 676.4 μ in thickness. The seed was put in the solution saturated with gypsum, then the solution was evaporated at the rate of 15 cc./day at 30°C. This evaporation rate was kept fairly constant by a special method. The evaporation was continued for 28 days until a small number of fine, needle-like precipitations began to appear on the bottom of the vessel. The final weight of the sample was 395.5 mg. This means the seed gained 196.2 mg. during the growth.

The grown seed is shown in *Photo* 7. There are many fine striations parallel to the c-axis on the surface and also many (101) faces at the edge. The outline of the original seed is seen clearly in the sample, showing that there is no growth in the a-axis direction. The outline of the sample as a whole is still irregular, but one may see a definite tendency of the shape of the grown seed of going toward the equilibrium form which consists of (101), (010), and (100) planes.

The overhanging (101) faces at the edge of the sample are common. The

overhangs take place at the edges of the both surfaces of the tabular sample, forming two parallel plates which extend themselves beyond the edge and are separated from each other by the distance corresponding to the width of the original seed.

Acknowledgement

The authors wish to thank Dr. Werner Lippert of Division of Building Research, CSIRO, Melbourne, and Associate Professor Dr. Saburo Uchiyama of Department of Mathematics, Hokkaido University, Sapporo, for their kind helps from mathematical point of view. Our thanks are also due to Professor Dr. Kenzo Yagi of Department of Geology and Mineralogy, Hokkaido University, for his valuable commemts and encouragement during this work. A large part of the calculations used in this paper were done with the electric computers in Calculation Center of Hokkaido University and also in Chemical Research Laboratory, CSIRO, Melbourne, and some part of them were done with the aid of the staffs of the calculation chamber in Division of Building Research, CSIRO. We are indebted to these staffs for their helpful cooperations. We also thank Mr. Shoichi Terada of Department of Minerelogy and Geology, Hokkaido University for his skilful assist in the preparation of this paper.

References

1. DANA, E. S.: The system of Mineralogy. (WILEY: New York, 1915).
2. KNOPP, K.: The Theory and Application of Infinite Series. (London, 1928).
3. WOOSTER, W. A: Z. KRIST, **94**, 375, (1936).

(Manuscript received Jan. 18, 1967)

PLATE 44 AND EXPLANATION

Explanation of Plate 44

Photo 1 An early stage of the growth of the $(\bar{1}01)$ cleaved step on the (010) surface of gypsum. Thin needles are seen running in the c-axis direction. ×100

Photo 2 Cracks parallel to the c-axis, which occurred in consequence of the dehydration of gypsum. ×10,000

Photo 3 Periodical distribution of rises on the $(\bar{1}01)$ cleaved step. ×10,000

Plate 44

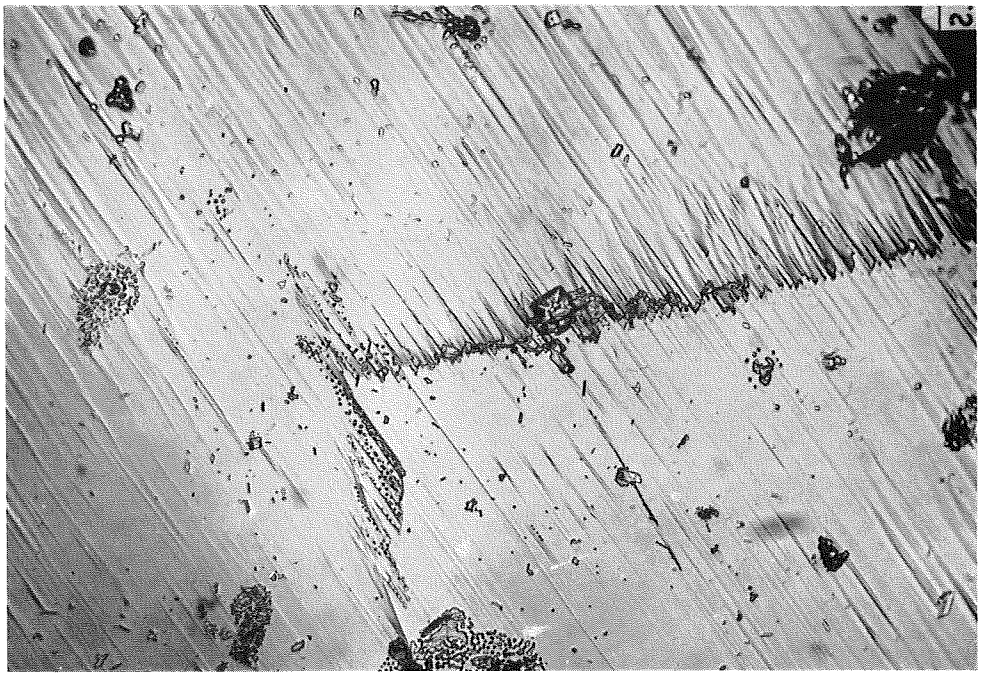

Photo 1

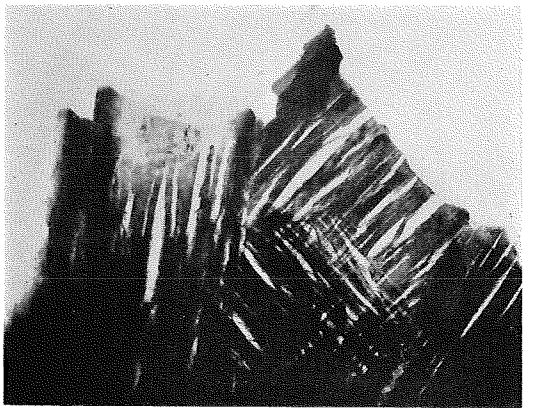

Photo 2

Photo 3

PLATE 45 AND EXPLANATION

Explanation of Plate 45

Photo 4 Needles starting from the $(\bar{1}01)$ cleaved step. They show the formations of the (601) and the (101) faces and also a very accute termination on their left sides. $\times 100$

Photo 5 Overhanging facets at the edge of the sample. $\times 100$

Plate 45

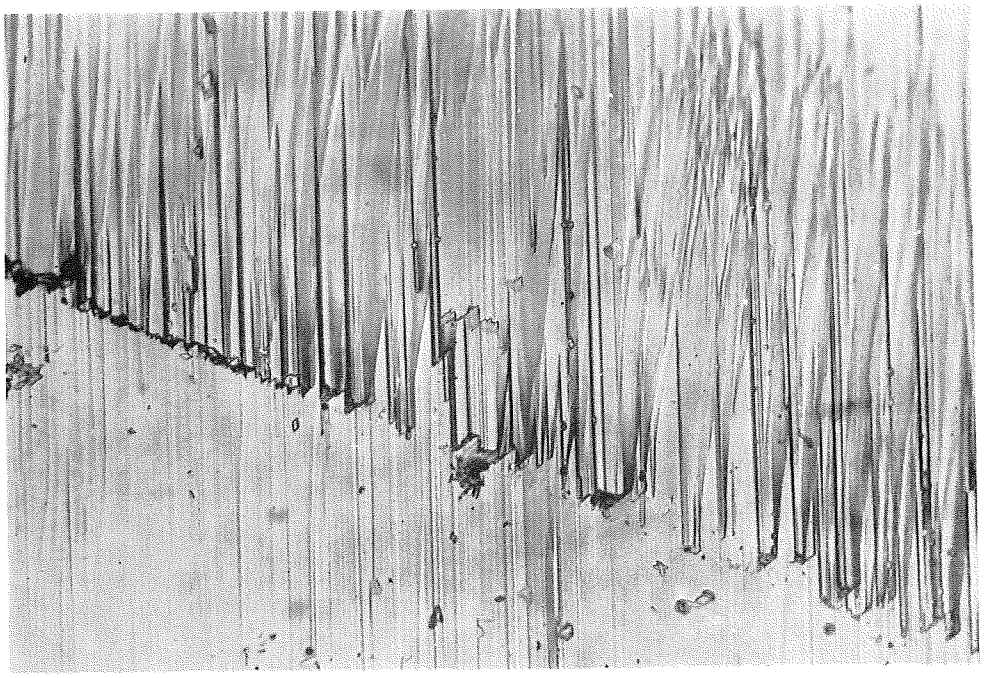

Photo 4

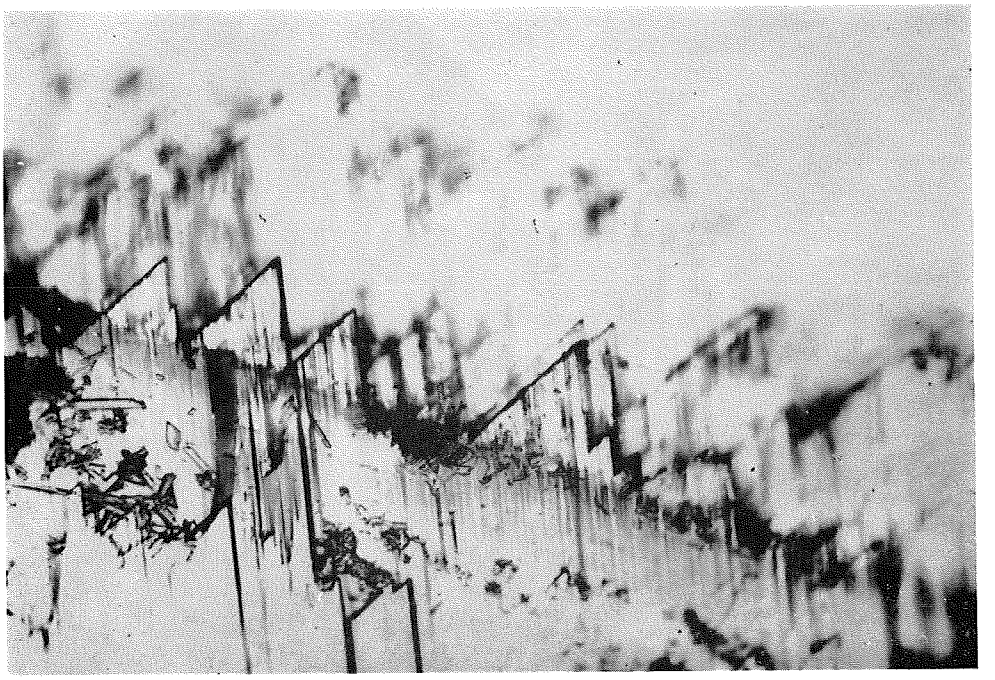

Photo 5

PLATE 46 AND EXPLANATION

Explanation of Plate 46

Photo 6 Narrow canal-like depressins running parallel to the C-axis on the growing (010) surface of gypsum ×100

Photo 7 Artificially grown seed of gypsum.

Plate 46

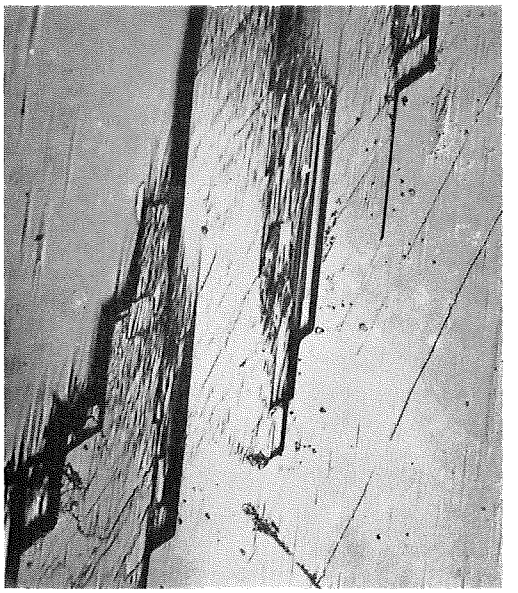

Photo 6

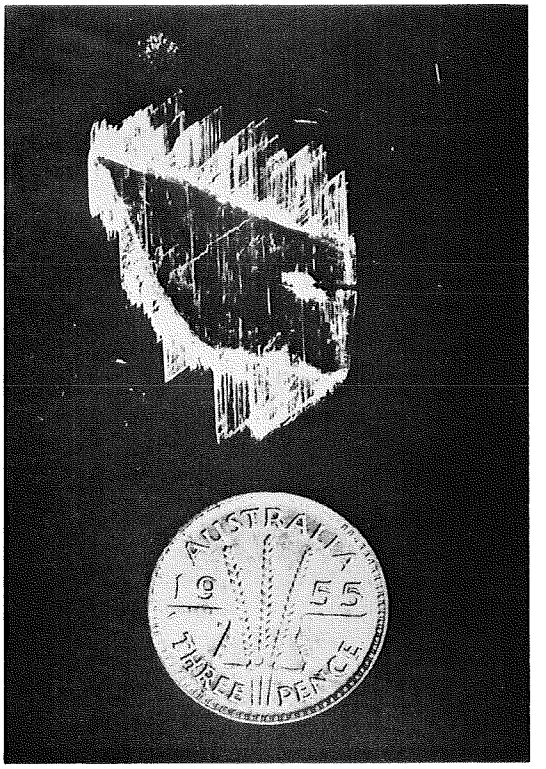

Photo 7